

Improved terahertz quantum cascade laser with variable height barriers

Alpar Matyas, Reza Chashmahcharagh, Istvan Kovacs, Paolo Lugli, Karun Vijayraghavan et al.

Citation: *J. Appl. Phys.* **111**, 103106 (2012); doi: 10.1063/1.4719071

View online: <http://dx.doi.org/10.1063/1.4719071>

View Table of Contents: <http://jap.aip.org/resource/1/JAPIAU/v111/i10>

Published by the [American Institute of Physics](#).

Related Articles

Buried-heterostructure quantum-cascade laser overgrown by gas-source molecular-beam epitaxy
Appl. Phys. Lett. **100**, 213504 (2012)

High power, continuous wave, room temperature operation of λ 3.4 μ m and λ 3.55 μ m InP-based quantum cascade lasers
Appl. Phys. Lett. **100**, 212104 (2012)

Thermal characterization of GaN-based laser diodes by forward-voltage method
J. Appl. Phys. **111**, 094513 (2012)

Model for direct-transition gain in a Ge-on-Si laser
Appl. Phys. Lett. **100**, 191113 (2012)

High-power 2.0 μ m semiconductor disk laser—Influence of lateral lasing
Appl. Phys. Lett. **100**, 192107 (2012)

Additional information on *J. Appl. Phys.*

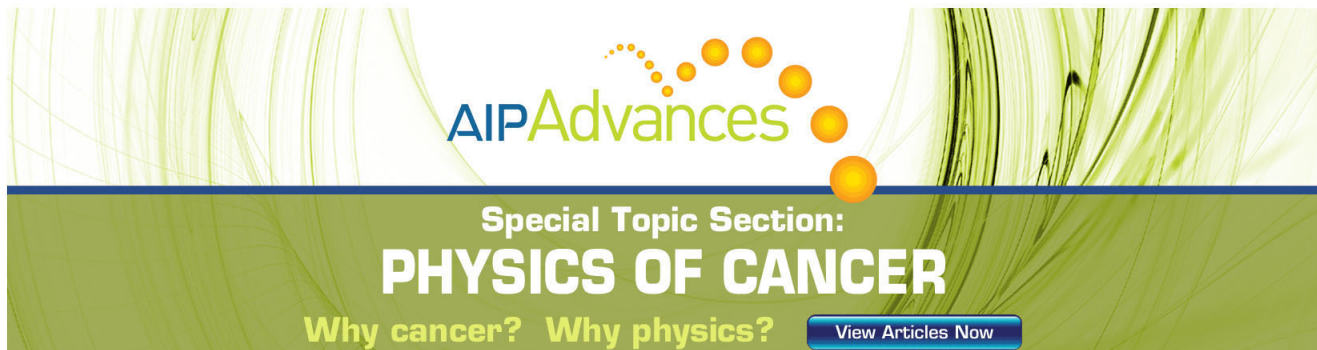
Journal Homepage: <http://jap.aip.org/>

Journal Information: http://jap.aip.org/about/about_the_journal

Top downloads: http://jap.aip.org/features/most_downloaded

Information for Authors: <http://jap.aip.org/authors>

ADVERTISEMENT

The advertisement features a green background with a pattern of thin, wavy lines. At the top, the 'AIP Advances' logo is shown, with 'AIP' in blue and 'Advances' in green, accompanied by a series of orange dots. Below the logo, the text 'Special Topic Section: PHYSICS OF CANCER' is displayed in white, with 'PHYSICS OF CANCER' in a larger, bold font. At the bottom, the phrase 'Why cancer? Why physics?' is written in yellow, and a blue button with the text 'View Articles Now' is located on the right side.

AIP Advances

Special Topic Section:
PHYSICS OF CANCER

Why cancer? Why physics? [View Articles Now](#)

Improved terahertz quantum cascade laser with variable height barriers

Alpar Matyas,^{1,2,a} Reza Chashmahcharagh,^{1,2} Istvan Kovacs,³ Paolo Lugli,²
Karun Vijayraghavan,⁴ Mikhail A. Belkin,⁴ and Christian Jirauschek^{1,2}

¹*Emmy Noether Research Group "Modeling of Quantum Cascade Devices," Technische Universität München, D-80333 Munich, Germany*

²*Institute for Nanoelectronics, Technische Universität München, D-80333 Munich, Germany*

³*Department of Electrical Engineering, Technical University of Cluj-Napoca, Cluj-Napoca, CJ RO-400027, Romania*

⁴*Department of Electrical and Computer Engineering, The University of Texas at Austin, Austin, Texas 78758, USA*

(Received 24 January 2012; accepted 12 April 2012; published online 21 May 2012)

Using an ensemble Monte-Carlo analysis, it is found that relaxing the constraint of identical barrier heights can result in an improved temperature performance. Exploiting this additional design degree of freedom, modified structures with non-uniform barrier heights are developed based on the current record temperature design. For an optimized structure with reduced diagonality, we predict an increase of 31 K for the maximum operating temperature. Furthermore, we develop improved designs with the same oscillator strength as for the reference design. Using a genetic algorithm for optimization, an improvement of the maximum operating temperature by 38 K is obtained. These results aim to show the potential of varying the barrier heights for the design of high temperature performance terahertz quantum cascade lasers. © 2012 American Institute of Physics. [<http://dx.doi.org/10.1063/1.4719071>]

I. INTRODUCTION

Quantum cascade lasers (QCLs) have gone through a remarkable progress in the past two decades, reaching continuous wave room temperature operation, increased wallplug efficiencies (WPEs), and high output powers in the midinfrared regime. In contrast, progress has been relatively slow for terahertz QCLs. The best performing designs up to date are based on resonant phonon depopulation of the lower laser state.¹ They are implemented in the GaAs/AlGaAs material system, mainly using 15% aluminium concentration in the barriers. Although some progress has been made during recent years,^{2–4} their operation is still limited to cryogenic temperatures, and the current record of 199.5 K (Refs. 4 and 5) is well below the thermoelectric cooling range, which is around 240 K. Another approach relies on difference frequency generation, using the output of two detuned midinfrared QCLs. Here, the optical nonlinearity can be integrated into the active region of one of the midinfrared QCLs,^{6–8} or included in a separate passive section.⁹ The main limitation of these structures is the microwatt-level output power due to the poor conversion efficiency.

All the recent record temperature terahertz QCLs (Refs. 2–4) are based on the three quantum well resonant phonon design.¹⁰ While the layer sequence has just been slightly varied, much of the improvement in the temperature performance has been due to a reduction of the waveguide losses. The introduction of additional design degrees of freedom can be helpful for a further improvement of the active region without having to abandon the well-established three well

design. In this paper, we aim at improving the temperature performance by relaxing the constraint of identical barrier heights within the QCL period. This is motivated by a number of previous works on both terahertz and midinfrared structures. Recently, it has been demonstrated that an increased barrier height can lead to a reduction of the threshold current density of bound to continuum terahertz QCLs, due to a weaker coupling of the intersubband states.¹¹ It has also been shown that three-well terahertz QCLs with good internal quantum efficiencies and very low threshold currents can be realized by using step wells.¹² For the case of midinfrared structures, deep well QCLs with varying barrier compositions have been developed for the suppression of thermal excitation of electrons to the X-valley and continuum states.^{13,14} This has considerably improved the performance of midinfrared QCLs, resulting in a more temperature-insensitive continuous wave operation and higher wallplug efficiency. It has also been shown theoretically that deep-well QCLs are more temperature insensitive,¹⁵ and wallplug efficiencies greater than 20% per facet have been projected.¹⁵ Other groups have taken a different approach: namely to add thin higher barriers in the center of the active region barriers, resulting in improved wallplug efficiency¹⁶ and temperature performance¹⁷ as well as reduced threshold current density.^{18,19} Motivated by these findings, we aim to investigate possible improvements in the temperature performance of terahertz QCLs by allowing for barriers with different material compositions within the structure, thus adding further design degrees of freedom.

Starting from the best performing terahertz QCLs to date,^{2–5} we develop strategies to optimize the temperature performance by varying the Al concentration in the barriers. For our analysis, we use a semiclassical ensemble

^aElectronic mail: alparmat@mytum.de. URL: <http://www.nano.ei.tum.de/noether>.

Monte-Carlo (EMC) method specifically developed for the modeling of such devices.^{20–22} The EMC method is based on the Boltzmann transport equation,²³ where scattering is self-consistently included using Fermi's golden rule. This approach has been successfully used for the analysis of the carrier transport^{24–31} and the lasing action^{32–34} in QCLs, as well as for the design^{24,35,36} of improved structures.

All the relevant mechanisms like electron (e)-longitudinal optical (LO) phonon, e-acoustic phonon, e-interface roughness (IR), e-impurity, and e-e scattering are routinely considered in our simulation tool. The spectral gain has been included based on lifetime broadening, which has been shown to yield valid results in reasonable agreement with experiment.²⁰ Space charge effects are considered by performing iterative Schrödinger-Poisson and EMC carrier transport simulations, and screening is implemented in the random phase approximation.^{22,30}

In semiclassical approaches such as EMC, the carrier transport between the subbands is described by semiclassical scattering rates, i.e., quantum coherence effects such as tunneling or quantum mechanical dephasing are not included. While in mid-infrared QCLs, such effects were found to be negligible,³⁷ they can play a more pronounced role in THz structures, where the energetic spacing between the quantized levels is closer.^{38,39} Quantum mechanical carrier transport approaches such as the density matrix^{37,40–43} and the nonequilibrium Greens function (NEGF) method^{44–46} routinely include such effects. However, the numerical complexity is largely increased, making approximations necessary to enable efficient QCL design.⁴⁷ This includes one-dimensional descriptions which do not account for intrasubband processes,^{40–42} or neglecting the momentum dependence of scattering mechanisms.⁴⁴ Furthermore, e-e scattering is routinely neglected. On the other hand, special care has to be taken in semiclassical EMC methods to avoid simulations at narrow anticrossing, where quantum coherence effects and dephasing can significantly influence the carrier transport, leading to spurious EMC simulation results.^{21,25} However, it has been shown that if narrow anticrossings are avoided, the EMC method yields valid results in good agreement with experiment,^{20,26,31} especially in the technically important lasing regime where incoherent scattering plays an important role.²¹ The reference THz QCL device,⁴ as well as the designed structures, all have their narrowest anticrossing (injection anticrossing) around 2.9 meV. This is well above the value of about 2 meV, where the EMC method starts to overestimate the experimental current and provides unphysical results for the investigated structures. For example, the current density found in EMC simulations of the reference structure agrees to within 10%-15% to the experimental value.⁴

For the further validation of our method, we show EMC simulation results for the last three record temperature terahertz QCLs, operating up to 178 K (Ref. 2) (2008), 186 K (Ref. 3) (2009) and 199.5 K (Refs. 4 and 5) (2012), respectively. In Fig. 1, the temperature dependence of their peak gain is given. All these structures are based on the three quantum well resonant phonon design.¹⁰ The vertical line is set to the simulated maximum gain of the 178 K design at its maximum operating temperature T_{\max} , thus indicating the

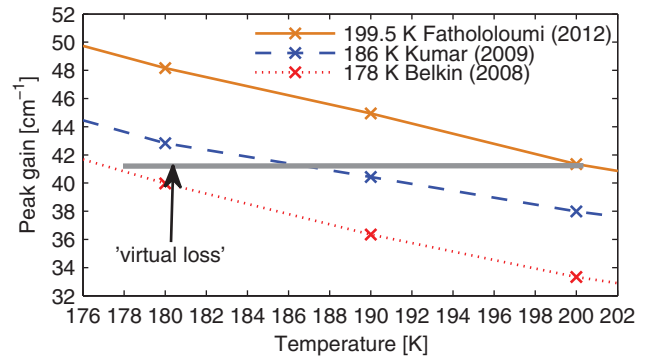


FIG. 1. Comparison of the temperature performance for various record temperature terahertz structures. The horizontal line is set to the gain at 178 K, the solid and dashed curves are corrected for the differences in resonator losses of the structures.

resonator loss of this structure. Differences in the resonator losses, originating from the removal of the top contact^{4,5,48,56} as well as from differences in the doping level⁴⁹ and operating frequency,⁵⁰ are taken into account by correcting the gain curves for the 186 K and 199.5 K structures. The simulation results show a quantitative agreement with the reported experimental maximum operating temperatures T_{\max} for the structures. The peak gain of the three structures was found to be at similar bias conditions, which is just before the roll-off to the negative differential resistance region.

II. IMPROVED DESIGNS

A. Increased lasing oscillator strength

Starting from the 199.5 K record structure, a further improvement of the temperature performance was targeted by allowing for different barrier heights. Our design strategy was as follows: The diagonality of the structure was somewhat reduced, leading to an increase of the lasing transition oscillator strength and thus to an enhanced optical gain. A reduced diagonality commonly results in increased leakage from the upper laser level and thus in a reduced population inversion, which counteracts the improvement obtained by the increased oscillator strength.³⁶ This detrimental effect could here be prevented by allowing for barriers with different heights within a period. Taking advantage of this additional design degree of freedom, a degradation of the inversion could be avoided by improving the injection and extraction efficiency, respectively. Two different strategies have been investigated, here referred to as injector-decoupled (ID) design (Fig. 2(a)) and scattering barrier (SB) design (Fig. 2(b)), respectively. An optimum value exists for the injection anticrossing in three well resonant phonon designs.⁵¹ Thus, we have kept this anticrossing at the reference value of the 199.5 K structure^{4,5} in our design process by adapting the injection barrier thickness. By contrast, no optimum value has been experimentally found for the extraction anticrossing in the investigated parameter range.⁵² Hence, we decided not to constrain the extraction barrier thickness. However, the barrier has been adapted to keep the anticrossing between injection and extraction

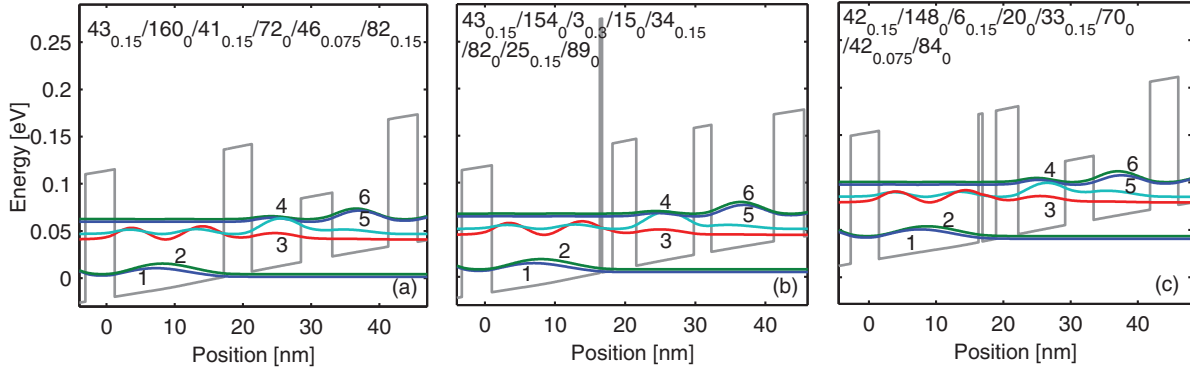


FIG. 2. Improved three quantum well designs: Conduction band profile and probability densities of the (a) ID scheme, (b) SB scheme, and (c) merged structure. In the figure plots, the layer sequence is given in Å, where the subscript represents the Al concentration in the $\text{Al}_x\text{Ga}_{1-x}\text{As}$ layer. The 50 Å mid-region of the injector well is doped with a sheet density of $3 \times 10^{10} \text{ cm}^{-2}$.

levels at the reference value of the 199.5 K structure, since this channel has been found to contribute to the parasitic current.⁴² Based on extracted data from our EMC simulations at 200 K and at the peak gain, we now explain the improvement of our designs resulting from the choice of different barrier heights.

The ID design in Fig. 2(a) aims at improving the injection into the upper laser level. The goal is to improve the temperature performance while keeping the phonon well and injection/extraction barriers the same as in the reference designs, to ensure that the physics in the new design is not very different and controllable. The width of the middle barrier in the lasing double well is increased while its height is reduced. This increases the spatial separation between the injector state 6 and levels 3 and 4. In this way, the parasitic injection from state 6 to levels 3 and 4 is reduced, and the electrons are redirected to the upper laser level 5, thus the injection efficiency into the upper laser level is improved. This becomes also clear from Table I. Here, some properties of the designed structures in this paper are listed at 200 K and at their peak current. We can see a large improvement of the injection efficiency for the ID structure ($\eta_5 = 53.6\%$) as compared to the reference ($\eta_5 = 45.3\%$). Furthermore, the reduced barrier height in the lasing double well leads to a

decrease in IR scattering from states 5 and 6 to 4. This, in turn, also compensates for the increased thermally activated scattering between these levels due to their increased oscillator strength.^{3,36} The EMC simulations at 200 K show that for the ID design, the occupations are nearly identical as in the 199.5 K reference design^{4,5} (see Table I). We also find that the gain bandwidths are very similar (within 2%). However, due to the 18% increased oscillator strength in the ID design, the peak gain is enhanced, and the simulation predicts an increase of T_{max} by about 16 K for this modified structure (Fig. 3, dashed line).

The SB design in Fig. 2(b) aims to improve the extraction from the lower laser level. Here, an additional high and thin barrier is introduced in the large injection well, which increases the net IR scattering from the lower laser level 4 to the extraction level 3, improving the depletion of the lower laser level. This approach is conceptually similar to the one recently proposed for mid-IR QCLs to facilitate electron extraction from the active region to the injector.⁵⁴ Since IR scattering is an elastic process, it tends to equalize the carrier distributions in the levels. Due to the higher population of level 4, this mechanism induces an increased net scattering to level 3. The amount of IR scattering is proportional to the square of the barrier height, thus higher barriers provide better extraction. On the other hand, the scattering rate depends on the product of the wavefunction values at the interface,

TABLE I. Summary for the properties of the designed structures at 200 K as compared to the reference design (199.5 K record structure⁴). The populations for the different levels (p_4 , p_5 , and p_6), the injection efficiencies into the upper and lower laser level (η_5 and η_4), the maximum current density (J), the total ($f_{\text{osc}}^{\text{tot}} = f_{\text{osc}}^{54} + f_{\text{osc}}^{64}$) and main lasing transition (f_{osc}^{54}) oscillator strength and the gain bandwidths (BW) are compared. Precise definitions for η_i can be found in Ref. 53.

	ID	SB	Merged	2BC	3BC	Reference
p_6 (%)	32.3	31.8	31.4	35.7	35.4	32.3
p_5 (%)	39.1	39.4	37.6	40.5	39.8	39.8
p_4 (%)	15.9	15.4	17.4	12.1	12.9	14.7
η_5 (%)	53.6	51.3	47.1	47	51.6	45.3
η_4 (%)	33.7	32	29.9	27.2	25.9	33.4
J (kA/cm ²)	1.766	1.718	2.016	1.605	1.575	1.651
$f_{\text{osc}}^{\text{tot}}$	0.748	0.678	0.952	0.57	0.606	0.615
f_{osc}^{54}	0.381	0.33	0.513	0.326	0.374	0.308
BW (THz)	1.584	1.588	1.555	1.572	1.553	1.622

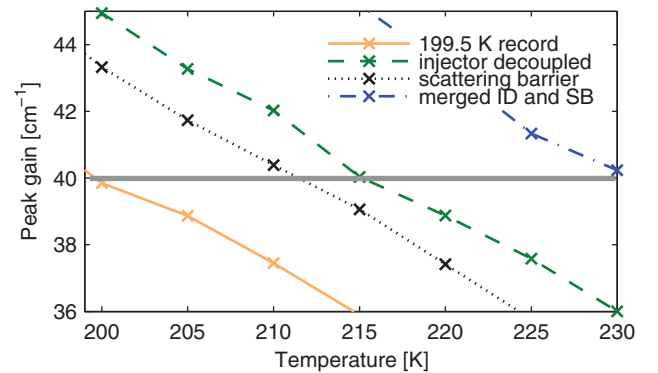


FIG. 3. Simulated temperature dependent peak gain of the structures, showing an improvement in T_{max} of about 16 K for the ID, 11 K for the SB, and 31 K for their merged design.

which is reduced for large barrier heights. This effect can be compensated by making this additional barrier thin. Furthermore, the additional barrier helps to localize state 3 in the wide injection well, which decreases overlap with states 5 and 6 and thus parasitic transitions to 3. To verify the improvements due to the additional barrier, the SB design has been compared to the reference structure,^{4,5} assuming moderate values for IR in our EMC simulation.²² The results indicate that the inversion in the SB structure gets slightly reduced, and the gain bandwidths are found to be identical to within 2% (see Table I). Thus, an improvement of T_{\max} by about 11 K is obtained for the SB design due to the increased oscillator strength (Fig. 3, dotted line).

As compared to the reference design, the improvements in the modified structures are obtained in different ways. We now discuss some of the improved quantities of the structures at 200 K at the bias of the maximum current. The upper laser level occupation, which is found to be about 39% for both designs, depends on the injection efficiency into the upper laser level η_5 as well as the leakage from the upper laser level to lower-lying states.⁵³ For the ID QCL, $\eta_5 = 53.6\%$ is obtained, as compared to 51.3% for the SB structure, which shows its superior injection. The lower laser level occupation is found to be similar for both designs. Here, the parasitic injection into the lower laser level is somewhat smaller for the SB design (see Table I); furthermore, the SB structure exhibits a reduced leakage from the upper to the lower laser level and an improved extraction.

As a next step, we have merged the improved designs into a single structure, combining the enhanced injection into the upper laser level of the ID QCL and the improved extraction from the lower laser level of the SB QCL. The design process was similar as described above: First, the diagonality of the reference structure^{4,5} was reduced to increase the lasing transition oscillator strength by 35%. Then, the modifications of both the injector decoupled design and the scattering barrier design were implemented to restore the inversion between the upper and lower laser level. Again, care was taken to keep the injector anticrossing to within 10% of the value for the reference structure; also the anticrossing 6-3 is only slightly increased (~ 0.1 meV). According to our EMC simulations, the current at the alignment bias of the anticrossing 6-3 rises only slightly by about 2% as compared to the reference structure, indicating that this parasitic channel has not become stronger in the merged design. In contrast, the current at the peak gain increases from 1.65 kA/cm^2 to 2.02 kA/cm^2 for the merged structure. Additionally, we observe an increase of the injection efficiency and decrease of the parasitic injection into the lower laser state, as shown in Table I. The EMC simulation results indicate that the inversion at 200 K is slightly reduced for the merged design as compared to the record structure. Furthermore, the gain bandwidth is found to be comparable, having slightly decreased by 4% from 1.622 THz to 1.555 THz. However, due to the 35% increased oscillator strength in the merged design, the peak gain is considerably enhanced (Fig. 3, dash-dotted line). The simulation results indicate an increase in T_{\max} by about 31 K for this improved structure. These findings suggest that by merging the modifications of the ID and

the SB design into a single structure, the improvements of both designs can be combined in a single device.

B. Optimized structures with preserved oscillator strength

In Sec. II A, we presented GaAs/AlGaAs QCL designs with different barrier compositions that have higher laser transition oscillator strength and similar population inversion, compared to the current state-of-the-art.^{4,5} In this section, we demonstrate that, by allowing for barriers with different material compositions within the structure, one may also create THz QCL designs with similar oscillator strength and higher population inversion, compared to the current state-of-the-art designs.^{4,5} In both cases, improvements lead to a higher value of T_{\max} for the proposed structures. For the design development, we proceeded as follows: First the barrier heights of the reference structure were changed, aiming for an improvement as discussed below for each of the optimized designs. Subsequently, the optimum layer thicknesses were determined using the standard genetic algorithm toolbox of the MATLAB software package. For each QCL layer, a limit for the upper and lower thickness was defined and the layers were varied by at least 1 Å. The goal here was to show that even with similar oscillator strengths and transition frequencies as in the reference structure, an improvement could be obtained due to the changed shape of the wavefunctions, leading to reduced parasitic injection into the lower laser level and increased injection efficiency into the upper laser level. Consequently, the minimization function was defined as

$$f = \sum_{i,j} (1 - f_{ij}^{\text{des}} / f_{ij}^{\text{ref}})^2 + \sum_{i,j} (1 - \nu_{ij}^{\text{des}} / \nu_{ij}^{\text{ref}})^2, \quad (1)$$

where f_{ij}^{des} and f_{ij}^{ref} are the oscillator strengths of the designed and reference structure between states i and j . Furthermore, ν_{ij}^{des} and ν_{ij}^{ref} are the frequencies corresponding to f_{ij}^{des} and f_{ij}^{ref} , respectively. Only pairs of states i and j with an energetic spacing corresponding to 0–10 THz were taken into account. The extraction anticrossing here was not taken into account, since an optimum value could not be found experimentally (see Sec. II A). The above quantities were calculated from the wavefunctions obtained with a Schrödinger-Poisson solver.⁵⁵

The first improved design is shown in Fig. 4(a), where we allow for barriers with two different material compositions (2BC design). The layer sequence is given in the figure. Here, the heights of the middle barrier in the lasing double well and the extraction barrier were reduced and their widths enlarged. This results in an increased spatial extension of levels 3 and 4, thus leading to less parasitic scattering from the upper laser level 5 and injection level 6 (see reduction of the parasitic injection η_4 in Table I). This helps to increase the population inversion of these structures. Furthermore, the injection barrier height was increased to obtain a better confinement of states 5 and 6, thus leading to an improved injection efficiency (see Table I).

In Fig. 4(b), a further improved design is shown where three different barrier heights have been used (3BC design).

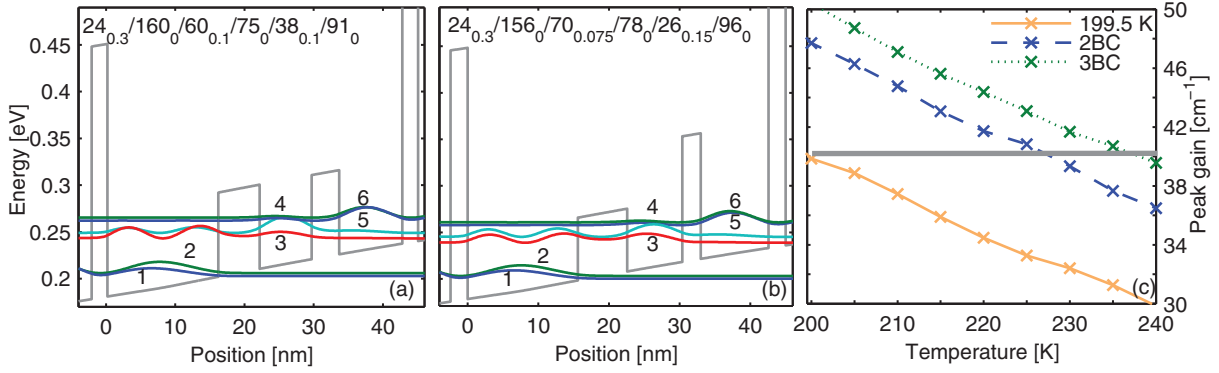


FIG. 4. Conduction band profile and probability densities for QCLs with the same oscillator strength as for the reference design with (a) two barrier compositions (2BC) and (b) three barrier compositions (3BC). The 50 Å mid-region of the injector well is doped with a sheet density of $3 \times 10^{10} \text{ cm}^{-2}$. (c) Simulated temperature dependent peak gain, showing an improvement in T_{max} of about 26 K for the 2BC design and 38 K for the 3BC design as compared to the reference structure.

Here, the extraction barrier height has been further reduced and its width enlarged, to increase the spatial extension of levels 3 and 4 even more, and thus further reduce the parasitic scattering from levels 5 and 6.

In the following, we discuss some of the quantitative improvements for the designed QCLs at 200 K and at the peak current. The main upper laser level populations (p_5) are approximately the same for these structures, however, the secondary upper laser level populations (p_6) are increased from 32.3% (reference) to 35.7% (2BC) and 35.4% (3BC). Furthermore, the lower laser level populations (p_4) are decreased from 14.7% (reference) to 12.1% (2BC) and 12.9% (3BC). The obtained results show that non-uniform barriers can lead to improved structures even if the oscillator strength is fixed to the value of the reference design. The higher population inversion in the improved structures results in an increased peak gain, as shown in Fig. 4(c). An improvement in T_{max} of about 26 K and 38 K is predicted for the 2BC and 3BC designs, respectively. The gain bandwidth of the improved structures is found to differ by only 3%–4% from the gain bandwidth of the reference design. Furthermore, the simulation provides a reduced current density of 1.605 kA/cm² and 1.575 kA/cm² for the 2BC and 3BC structure, respectively, as compared to 1.65 kA/cm² for the reference design. For the 3BC structure, the design bias is also reduced, as compared to the other designs. Together with the higher gain, this indicates improved WPE for the optimized structures, especially for the 3BC design. This is similar as in mid-IR structures, where alternating barriers were used to improve the WPE by reducing leakage to the continuum.¹³ Here, however, the WPE is improved rather by shaping the wavefunctions and thus reducing parasitic effects, in contrast to reducing the leakage to continuum.

III. CONCLUSION

In summary, we have demonstrated that relaxing the restriction of identical barrier heights in THz QCLs provides an additional design degree of freedom, which can be used to improve their temperature performance. Based on an EMC simulation tool which reproduces the measured maximum operating temperatures of recent experimental record

QCLs, modified structures have been developed, based on the current record temperature design.^{4,5} First, structures with an increased oscillator strength have been designed, yielding an overall improvement in T_{max} of 31 K as compared to the record structure. Second, based on a genetic algorithm, designs have been developed with similar oscillator strengths as the reference design, showing an improvement in T_{max} of up to 38 K.

ACKNOWLEDGMENTS

A.M. and C.J. acknowledge support from the Emmy Noether program of the German Research Foundation (DFG, JI115/1-1). Additionally, C.J. acknowledges funding by the Nanosystems Initiative Munich. A.M. thanks E. Dupont and S. Fathololoumi for fruitful discussions. M.A.B. acknowledges support from the NSF Grant No. ECCS-0935217 and the “Norman Hackerman Advanced Research Program” award.

- ¹Q. Hu, B. S. Williams, S. Kumar, H. Callebaut, S. Kohen, and J. L. Reno, *Semicond. Sci. Technol.* **20**, 228 (2005).
- ²M. A. Belkin, J. A. Fan, S. Hormoz, F. Capasso, S. P. Khanna, M. Lachab, A. G. Davies, and E. H. Linfield, *Opt. Express* **16**, 3242 (2008).
- ³S. Kumar, Q. Hu, and J. L. Reno, *Appl. Phys. Lett.* **94**, 131105 (2009).
- ⁴S. Fathololoumi, E. Dupont, C. W. I. Chan, Z. R. Wasilewski, S. R. Laframboise, D. Ban, A. Mátyás, C. Jirasek, Q. Hu, and H. C. Liu, *Opt. Express* **20**, 3866 (2012).
- ⁵C. W. I. Chan, S. Fathololoumi, E. Dupont, Z. R. Wasilewski, S. R. Laframboise, D. Ban, Q. Hu, and H. C. Liu, in *the 11th International Conference on Intersubband Transitions in Quantum Wells* (Le Dune Resort, Badesi, Sardinia Italy, 2011).
- ⁶M. A. Belkin, F. Capasso, A. Belyanin, D. L. Sivco, A. Y. Cho, D. C. Oakley, C. J. Vineis, and G. W. Turner, *Nat. Photonics* **1**, 288 (2007).
- ⁷M. A. Belkin, F. Capasso, F. Xie, A. Belyanin, M. Fischer, A. Wittmann, and J. Faist, *Appl. Phys. Lett.* **92**, 201101 (2008).
- ⁸Q. Y. Lu, N. Bandyopadhyay, S. Slivken, Y. Bai, and M. Razeghi, *Appl. Phys. Lett.* **99**, 131106 (2011).
- ⁹R. W. Adams, A. Vizbaras, M. Jang, C. Grasse, S. Katz, G. Boehm, M. C. Amann, and M. A. Belkin, *Appl. Phys. Lett.* **98**, 151114 (2011).
- ¹⁰H. Luo, S. R. Laframboise, Z. R. Wasilewski, G. C. Aers, H. C. Liu, and J. C. Cao, *Appl. Phys. Lett.* **90**, 041112 (2007).
- ¹¹M. Wienold, L. Schrottke, M. Giehler, R. Hey, W. Anders, and H. T. Grahn, *Appl. Phys. Lett.* **97**, 071113 (2010).
- ¹²G. Scalari, M. I. Amanti, M. Fischer, R. Terazzi, C. Walther, M. Beck, and J. Faist, *Appl. Phys. Lett.* **94**, 041114 (2009).

- ¹³J. C. Shin, M. D'Souza, Z. Liu, J. Kirch, L. J. Mawst, D. Botez, I. Vurgaftman, and J. R. Meyer, *Appl. Phys. Lett.* **94**, 201103 (2009).
- ¹⁴D. P. Xu, M. D'Souza, J. C. Shin, L. J. Mawst, and D. Botez, *J. Cryst. Growth* **310**, 2370 (2008).
- ¹⁵D. Botez, S. Kumar, J. C. Shin, L. J. Mawst, I. Vurgaftman, and J. R. Meyer, *Appl. Phys. Lett.* **97**, 071101 (2010).
- ¹⁶Y. Bai, N. Bandyopadhyay, S. Tsao, E. Selcuk, S. Slivken, and M. Razezghi, *Appl. Phys. Lett.* **97**, 251104 (2010).
- ¹⁷S. Katz, G. Boehm, and M.-C. Amann, *Electron. Lett.* **44**, 580 (2008).
- ¹⁸J. Shin, L. Mawst, D. Botez, I. Vurgaftman, and J. Meyer, *Electron. Lett.* **45**, 741 (2009).
- ¹⁹H. Li, S. Katz, G. Boehm, and M.-C. Amann, *Appl. Phys. Lett.* **98**, 131113 (2011).
- ²⁰C. Jirauschek and P. Lugli, *J. Appl. Phys.* **105**, 123102 (2009).
- ²¹A. Mátyás, T. Kubis, P. Lugli, and C. Jirauschek, *Physica E* **42**, 2628 (2010).
- ²²C. Jirauschek, A. Mátyás, and P. Lugli, *J. Appl. Phys.* **107**, 013104 (2010).
- ²³R. C. Iotti, E. Ciancio and F. Rossi, *Phys. Rev. B* **72**, 125347 (2005).
- ²⁴R. Köhler, R. C. Iotti, A. Tredicucci, and F. Rossi, *Appl. Phys. Lett.* **79**, 3920 (2001).
- ²⁵H. Callebaut, S. Kumar, B. S. Williams, Q. Hu, and J. L. Reno, *Appl. Phys. Lett.* **83**, 207 (2003).
- ²⁶H. Callebaut, S. Kumar, B. S. Williams, Q. Hu, and J. L. Reno, *Appl. Phys. Lett.* **84**, 645 (2004).
- ²⁷C. Jirauschek, G. Scarpa, P. Lugli, M. S. Vitiello, and G. Scamarcio, *J. Appl. Phys.* **101**, 086109 (2007).
- ²⁸X. Gao, D. Botez, and I. Knezevic, *J. Appl. Phys.* **101**, 063101 (2007).
- ²⁹X. Gao, M. D'Souza, D. Botez, and I. Knezevic, *J. Appl. Phys.* **102**, 113107 (2007).
- ³⁰J. T. Lü and J. C. Cao, *Appl. Phys. Lett.* **89**, 211115 (2006).
- ³¹H. Li, J. C. Cao, Y. J. Han, X. G. Guo, Z. Y. Tan, J. T. Lü, H. Luo, S. R. Laframboise, and H. C. Liu, *J. Appl. Phys.* **104**, 043101 (2008).
- ³²C. Jirauschek, *Appl. Phys. Lett.* **96**, 011103 (2010).
- ³³A. Mátyás, P. Lugli, and C. Jirauschek, *J. Appl. Phys.* **110**, 013108 (2011).
- ³⁴C. Jirauschek, *Opt. Express* **18**, 25922 (2010).
- ³⁵H. Li, J. C. Cao, and H. C. Liu, *Semicond. Sci. Technol.* **23**, 125040 (2008).
- ³⁶A. Mátyás, M. A. Belkin, P. Lugli, and C. Jirauschek, *Appl. Phys. Lett.* **96**, 201110 (2010).
- ³⁷R. C. Iotti and F. Rossi, *Phys. Rev. Lett.* **87**, 146603 (2001).
- ³⁸H. Callebaut and Q. Hu, *J. Appl. Phys.* **98**, 104505 (2005).
- ³⁹C. Weber, A. Wacker, and A. Knorr, *Phys. Rev. B* **79**, 165322 (2009).
- ⁴⁰S. Kumar and Q. Hu, *Phys. Rev. B* **80**, 245316 (2009).
- ⁴¹R. Terazzi and J. Faist, *New J. Phys.* **12**, 033045 (2010).
- ⁴²E. Dupont, S. Fatholouloumi, and H. C. Liu, *Phys. Rev. B* **81**, 205311 (2010).
- ⁴³C. Weber, F. Banit, S. Butscher, A. Knorr, and A. Wacker, *Appl. Phys. Lett.* **89**, 091112 (2006).
- ⁴⁴A. Wacker, *Phys. Rev. B* **66**, 085326 (2002).
- ⁴⁵T. Kubis, C. Yeh, P. Vogl, A. Benz, G. Fasching, and C. Deutsch, *Phys. Rev. B* **79**, 195323 (2009).
- ⁴⁶T. Schmielau and M. F. Pereira, *Appl. Phys. Lett.* **95**, 231111 (2009).
- ⁴⁷T. Kubis and P. Vogl, *Phys. Rev. B* **83**, 195304 (2011).
- ⁴⁸The reported influence of the top contact layer in case of Au-Au waveguides is 15 K.^{4,5} Based on our EMC simulation at 180 K and 195 K, this corresponds to a loss of about 5.5 cm^{-1} . However, the Drude model gives only a slight change of 1 cm^{-1} .^{4,5} The strong effect of the top contact layer observed in the experiment could be due to diffusion of the dopants from this layer into the first few periods of the QCL, which limits the operation and increases the loss further (Refs. 4, 5, and 56).
- ⁴⁹The QCL from Ref. 2 has a sheet doping density of $2.75 \times 10^{10} \text{ cm}^{-2}$ while the other structures have $3 \times 10^{10} \text{ cm}^{-2}$. For metal-metal waveguides, the resonator loss scales linearly with the doping. Based on EMC simulation results at 178 K, this corresponds to a reduction in resonator loss of about 3.5 cm^{-1} for the structure in Ref. 2, as compared to the other structures.
- ⁵⁰The QCL published by Kumar and coworkers operated at a slightly higher frequency, i.e., lower waveguide loss by about 1.5 cm^{-1} estimated from Fig. 1 in Ref. 2.
- ⁵¹H. Luo, S. Laframboise, Z. Wasilewski, and H. Liu, *Electron. Lett.* **43**, 633 (2007).
- ⁵²H. Luo, S. Laframboise, Z. Wasilewski, H. Liu, and J. Cao, *Electron. Lett.* **44**, 630 (2008).
- ⁵³C. Jirauschek and P. Lugli, *Phys. Status Solidi C* **5**, 221 (2008).
- ⁵⁴Y. Chiu, Y. Dikmelik, J. B. Kurgin, and C. Gmachl, in *the 11th International Conference on Intersubband Transitions in Quantum Wells* (2011).
- ⁵⁵C. Jirauschek, *IEEE J. Quantum Electron.* **45**, 1059 (2009).
- ⁵⁶S. Kumar, "Development of Terahertz Quantum-Cascade Lasers," Ph.D. dissertation (Department of Electrical Engineering and Computer Science, Massachusetts Institute of Technology, Cambridge, MA, 2007).